



**HAL**  
open science

## Unravelling water effects on solid acidic catalysts: Case study of TiO<sub>2</sub> /SiO<sub>2</sub> for dehydration of isobutanol

Zoé Buniagnet, Julien Couble, Daniel Bianchi, Mickael Rivallan, Amandine Cabiac, Sylvie Maury, Stéphane Loridant

### ► To cite this version:

Zoé Buniagnet, Julien Couble, Daniel Bianchi, Mickael Rivallan, Amandine Cabiac, et al.. Unravelling water effects on solid acidic catalysts: Case study of TiO<sub>2</sub> /SiO<sub>2</sub> for dehydration of isobutanol. Journal of Catalysis, 2017, 348, pp.125-134. 10.1016/j.jcat.2016.12.007 . hal-01566161

**HAL Id: hal-01566161**

**<https://ifp.hal.science/hal-01566161>**

Submitted on 20 Jul 2017

**HAL** is a multi-disciplinary open access archive for the deposit and dissemination of scientific research documents, whether they are published or not. The documents may come from teaching and research institutions in France or abroad, or from public or private research centers.

L'archive ouverte pluridisciplinaire **HAL**, est destinée au dépôt et à la diffusion de documents scientifiques de niveau recherche, publiés ou non, émanant des établissements d'enseignement et de recherche français ou étrangers, des laboratoires publics ou privés.

**Unravelling water effects on solid acidic catalysts:  
Case study of TiO<sub>2</sub>/SiO<sub>2</sub> for dehydration of isobutanol**

Z. Buniazet<sup>1,2</sup> J. Couble,<sup>1</sup> D. Bianchi,<sup>1</sup> M. Rivallan,<sup>2</sup> A. Cabiac,<sup>2</sup> S. Maury,<sup>2</sup> S. Loridant<sup>1,\*</sup>

<sup>1</sup> *Institut de Recherches sur la Catalyse et l'Environnement de Lyon, IRCELYON, CNRS-  
Université Claude Bernard Lyon 1, 2 av. Einstein, F-69626 Villeurbanne Cedex, France*

<sup>2</sup> *IFP Energies nouvelles, BP 3, F-69360 Solaize, France*

\* Corresponding Author: Ph. + 33 [0] 472 445 334, Fax + 33 [0] 472 445 399, E-mail [stephane.loridant@ircelyon.univ-lyon1.fr](mailto:stephane.loridant@ircelyon.univ-lyon1.fr)

## Abstract

The understanding of water effects on acidic catalysts is key issue to develop efficient process producing olefins from bio-alcohols. In this work, the water effects on TiO<sub>2</sub>/SiO<sub>2</sub> catalysts used for the gas phase conversion of isobutanol into linear olefins have been unraveled. Such compounds prepared by grafting on mesoporous SiO<sub>2</sub> contained well dispersed TiO<sub>2</sub> amorphous clusters anchored by Ti-O-Si linkages leading to much higher catalytic activity than TiO<sub>2</sub> and SiO<sub>2</sub>. Furthermore, addition of water into the feed was shown to significantly improve it. Acidity measurements indicated that TiO<sub>2</sub>/SiO<sub>2</sub> mixed oxides were mostly of Lewis type after activation at 450°C. However, *in situ* acidity measurements achieved, for the first time, flowing NH<sub>3</sub> probe and water vapor at the reaction temperatures, showed that the amount of Lewis sites remained constant while weak Brønsted sites were formed and corresponded to active sites. Their hydrolysis generated OH acidic groups leading to catalytic activity enhancement under H<sub>2</sub>O.

**Keywords:** acidic catalyst, water effects, *in situ* acidity measurements, bioalcohols, olefins, dehydration

## 1. Introduction

Olefins which represent key chemicals for polymers industry are presently produced by petrochemical routes. Among C4 olefins, 1-butene is obtained by dimerization of ethylene and the others (cis-2-butene, trans-2-butene and isobutene) by fluid catalytic cracking or steam cracking of naphtha [1]. Dehydration of bio-alcohols represents a sustainable alternative route for olefins production. Indeed, ethanol and n-butanol can be now synthesized in large volumes by metabolic and engineered pathways [2-6]. Furthermore, new biochemical routes have been developed to produce selectively isobutanol from carbohydrates, from syngas by a Fischer-Tropsch process and Guerbet condensation of methanol and ethanol which can be bio-sourced [7-9].

However, the acid catalysts developed for petrochemistry and which can yield such reactions are usually not suitable because water present in bio-alcohols and generated by their dehydration often gives rise to lower activity and deactivation [7,10-12]. Therefore, the discovering of efficient catalysts, stable in the presence of water, represents a major challenge. For that purpose a full understanding of water effects in reaction conditions is required. Water can modify the catalytic activity of acid catalysts by:

- Irreversible textural and/or structural evolutions [12,13],
- Reactant solvation [14] or competitive adsorption leading to a decrease in the number of catalytic sites [7,10],
- Products dilution or solvation limiting consecutive reactions and coke formation [15,16],
- Altering the nature of sites: for instance, Lewis acid sites can adsorb and dissociate water leading to their conversion into Brønsted acid sites and hydroxylation while the so called 'water tolerant' Lewis sites correspond to the unconverted ones [17-21]. Conversion of Lewis to Brønsted sites would occur only in liquid but not in gas phase [22,23].

Contradictions can be found in the literature because the above-listed effects can occur simultaneously, because they depend on the catalyst and the reaction conditions and because most of studies were achieved *ex situ* whereas *in situ* measurements are required for understanding. In this work, *in situ* acidity measurements achieved in flowing water vapor at the reaction temperatures were achieved to unravel the water effects on TiO<sub>2</sub>/SiO<sub>2</sub> catalysts used for the gas phase dehydration of isobutanol into olefins. In this case, water was formed

by the reaction itself and was added or not to the feed. The catalysts prepared by grafting on mesoporous SiO<sub>2</sub> were also characterized in details by structural (XRD, Raman, TEM, XPS), textural (liquid N<sub>2</sub> adsorption) techniques and classical acidity measurements using four different probes.

## 2. Experimental part

### 2.1 Catalysts preparations

The preparation of TiO<sub>2</sub>/SiO<sub>2</sub> catalysts was adapted from a reported method [24] grafting Ti(OiPr)<sub>2</sub>(OC<sub>5</sub>H<sub>10</sub>)<sub>2</sub> over SiO<sub>2</sub>. For that purpose, Ti(OiPr)<sub>4</sub> precursor was dissolved in 5 mL of dry isopropanol. In a dry box under N<sub>2</sub> flow, 1 molar equivalent of Ti(OiPr)<sub>4</sub> was then stirred for 20 min with 6 molar equivalent of C<sub>5</sub>H<sub>8</sub>O<sub>2</sub>. Various masses of silica provided by Evonik (Grace or Aerosil 200) were desorbed at 300 °C for 2 h under vacuum of 10<sup>-5</sup> Pa and then poured into 10 mL of dry isopropanol under magnetic stirring. After mixing the two solutions for 6 h, the color changed from orange to pale yellow indicating complete reaction. The solid was then recovered using rotavapor, dried at 110 °C overnight and calcined under air flow for 6 h at 425 °C. The latter temperature was chosen from TGA/TDA measurements indicating complete decomposition of organic compounds. In the following, the prepared compounds are labeled x%TiO<sub>2</sub>/SiO<sub>2</sub>-G (or A) where x corresponds to the weight percent of TiO<sub>2</sub>, G or A indicated if the Grace or Aerosil support was respectively used. Bulk TiO<sub>2</sub> sample was purchased from Degussa (P25, anatase and rutile mixture, ca 50 m<sup>2</sup>.g<sup>-1</sup>). It is labeled TiO<sub>2</sub>-P25 in the following.

### 2.2 Catalysts characterization

Structural characterization was obtained crossing X-rays diffraction (XRD), Raman spectroscopy and Transmission Electronic Microscopy (MET). XRD patterns were achieved between 5 and 80° (2θ) on a Bruker D8 Advance A25 diffractometer equipped with a Ni filter (Cu K<sub>α</sub> radiation: 0.154184 nm) and a one-dimensional multistrip detector (Lynxeye, 192 channels on 2.95°). The International Center for Diffraction Data (ICDD) library was used for phase identification and Bruker Topas P program for quantification of the phases identified. Raman spectra were recorded with a LabRam HR Raman spectrometer (Horiba-Jobin Yvon). The exciting laser at 514 nm of an Ar laser was focused using a ×50 long working distance objective. The influence of the laser power on spectra was previously investigated and a value of ca 1 mW was chosen to avoid heating effect. Mappings achieved on 90 different analysis areas revealed high structural homogeneity at the micrometer scale. *In*

*situ* Raman spectra were recorded using a THMS600 cell (Linkam) at 450 °C in air. X-ray photoelectron experiments were carried out in a Kratos Axis Ultra DLD spectrometer. The spectra of the C 1s, O 1s, Ti 2p, Si 2p levels were recorded using the Al K $\alpha$  X-ray radiation (1486.6 eV), with pass energy of 20 eV and spot size aperture of 300 x 700  $\mu$ m. The binding energies were calibrated using the C 1s band of adventitious carbon at 284.6 eV. TEM images were achieved with a JEOL 2010 microscope. The acceleration voltage was 200 kV with LaB $_6$  emission current and the point resolution was 0.19 nm. Before measurements, a dispersion of catalyst crushed in ethanol was deposited on standard holey carbon-covered copper TEM grids.

Textural properties were obtained by nitrogen physisorption at -196 °C with a Micromeritics ASAP 2020 instrument applying the BET and BJH methods to determine the specific surface areas ( $S_{\text{BET}}$ ), both the pores volumes ( $V_{\text{pores}}$ ) and the pores diameters ( $D_{\text{pores}}$ ) respectively.

Acidity properties were probed by adsorption of CO, acetonitrile, pyridine and NH $_3$ . For all the measurements, self-supporting pellets (20-30 mg) were desorbed at 450 °C for 10 h under air flow which corresponded to the activation treatment before catalytic testings. Spectra of CO or acetonitrile adsorbed at -196 °C or RT respectively were obtained with a Vertex 702 (Bruker) spectrometer equipped with DTGS detector. Adsorption was performed by introducing small calibrated doses at increasing pressure. Pyridine adsorption experiments were performed with a static experimental setup under vacuum. A homemade IR cell equipped with KBr windows was used. After cooling at room temperature, pressure of 4 mbar of pyridine was introduced in contact to the activated sample. Transmission IR spectra of samples desorbed at increasing temperatures were then recorded at RT with Vector 22 (Bruker) spectrometer equipped with DTGS detector. The bands at 1446 and 1575 cm $^{-1}$  were chosen for quantification of Lewis and Brønsted acid sites densities using extinction coefficient values of 1.50 and 1.67 cm $\cdot\mu$ mol $^{-1}$ , respectively [25-27].

Finally, *in situ*-FTIR acidity measurements under NH $_3$  and/or water vapor flow ( $P_{\text{NH}_3}$  0-1%,  $P_{\text{H}_2\text{O}}$  0-3%) were achieved with Nicolet 6700 (ThermoScientific) spectrometer in a IR cell reactor specially designed to limit the gas phase contribution [28]. Indeed, its optical path of only 2.2 mm allowed relevant data to be obtained in the temperature range 293-800 K under water vapor [29].

### 2.3 Catalytic testing

Catalytic measurements were conducted at atmospheric pressure between 200 °C and 300 °C after pretreatment at 450 °C for 2 h under synthetic air flow (70 mL.min<sup>-1</sup>). Reaction parameters such as the temperature, the contact time, the time on stream and feed water addition were investigated. For that purpose, pure isobutanol or 7% H<sub>2</sub>O in isobutanol was sent with HPLC pump to a home-made vaporizer heated at 130 °C and then diluted with a CH<sub>4</sub>-N<sub>2</sub> mixture. CH<sub>4</sub> which was inert at the reaction temperatures was used as internal standard. The vaporization temperatures were previously determined for the H<sub>2</sub>O-iC<sub>4</sub>H<sub>9</sub>OH phase diagram simulated with ProSim software. The reaction mixture was kept at 130 °C to avoid condensation and sent to a straight fixed bed reactor heated by a tubular furnace. After the reactor, unreacted isobutanol, H<sub>2</sub>O and casual heavy products were condensed in trap containing ethanol cooled at 10 °C. A given mass of 1-propanol was added to the solution and used as an external standard. The overall solution was then analyzed off-line with GC-FID chromatograph (Shimadzu GC-2014) equipped with a Supelco column (30 m x 0.32 mm x 0.25 μm). C<sub>4</sub> olefins (trans 2-butene, cis 2-butene, 1-butene and isobutene) which were not trapped were analyzed on line with GC-FID chromatograph (Shimadzu GC-2014) equipped with an Agilent HP-AL/KCL column (30 m x 0,535 mm x 15 μm). The GC also allowed analysis of C<sub>1</sub> to C<sub>5</sub> hydrocarbons when present in the outlet gas mixture. TiO<sub>2</sub>/SiO<sub>2</sub> catalysts were also evaluated for conversion of isobutene. The same set up was used except that isobutene was directly diluted with a CH<sub>4</sub>-N<sub>2</sub> mixture using flowmeters. The feed composition was iC<sub>4</sub>H<sub>8</sub>/inert: 16/84 or iC<sub>4</sub>H<sub>8</sub>/H<sub>2</sub>O/inert: 16/10/74, 1/WHSV value ?? g.h.mol<sup>-1</sup> and the reaction temperature was varied from 300 to 450 °C. The formulas used to calculate the conversions, selectivity sets and the carbon balance were the following:

$$\text{Conversion (\%)} = 100 \times \frac{\text{moles of reactant in} - \text{moles of reactant out}}{\text{moles of reactant in}}$$

$$Y_{\text{product}} (\%) = 100 \times K \times \frac{\text{moles of product}}{\text{moles of reactant in}} \quad \text{with } K = \frac{\text{number of carbons in product}}{4}$$

$$\text{Carbon balance (\%)} = \sum \text{Yield} + 100 - \text{Conversion}$$

Carbon balance values between 95 and 105% were obtained for the catalytic measurements reported in the following which ensured high quality of the GC analyses. Furthermore, as only butenes were detected by GC (no dialkyl ether, no cracking and condensation product), the selectivity values were normalized using the formula:

$$S_{\text{product}} (\%) = 100 \times \frac{\text{moles of product}}{\sum \text{moles of butenes}}$$

Finally, the isomerization activity was related to the linear butenes selectivity defined by:

$$S_{\text{LinBut}} (\%) = \sum(S_{\text{trans 2 butene}} + S_{\text{cis 2 butene}} + S_{\text{1 butene}})$$

### 3. Results

#### 3.1 Characterization of the catalysts

A first goal of the study was to maximize the TiO<sub>2</sub> loading on SiO<sub>2</sub> while keeping amorphous and well dispersed titania. Figure 1 compares the XRD patterns of prepared compounds. For SiO<sub>2</sub>-G support, only a very broad band around 22.5° (2θ) appeared up to a TiO<sub>2</sub> loading of 20.4% which indicated that the various solids were amorphous. For SiO<sub>2</sub>-A support, a weak broad band around 25.2° was observed and indexed as the (101) plane of anatase TiO<sub>2</sub> [30,31]. Raman spectra of these compounds (Figure S1 in the Supporting Information) which contained bands around 151, 202 (shoulder), 401, 493, 510 and 640 cm<sup>-1</sup> clearly evidenced the presence of anatase nanocrystallites in these samples [32,33]. The very broad features around 460 and 810 cm<sup>-1</sup> corresponded respectively to δ(Si-O-Si) and ν(Si-O-Si) of SiO<sub>2</sub> support whereas the remaining band at 607 cm<sup>-1</sup> was attributed to D2 defects (3-membered rings) [34]. The significant blue-shift and broadening of the Eg band at 151 cm<sup>-1</sup> compared to single crystal of anatase was due to phonon confinement in TiO<sub>2</sub> nanocrystallites. [35]. Its wavenumber and its bandwidth (28-35 cm<sup>-1</sup>) suggested a crystallite size of ca 3-4 nm [36-38]. Furthermore, the BE values of the Ti 2p<sub>3/2</sub> peak of TiO<sub>2</sub>/SiO<sub>2</sub> solids were close to the one of TiO<sub>2</sub>-P25 (Table S1) which indicated that they contained mainly Ti<sup>4+</sup> cations with similar environment. The small blue-shift suggested the existence of Ti-O-Si bonds since Si has higher electronegativity than Ti [39,40]. Comparison of TEM images of 20.4%TiO<sub>2</sub>/SiO<sub>2</sub>-G and 19.5%TiO<sub>2</sub>/SiO<sub>2</sub>-A showed high dispersion of TiO<sub>2</sub> domains which were amorphous for the most part while some of them were nanocrystallized (Figure 2). For 19.5%TiO<sub>2</sub>/SiO<sub>2</sub>-A, the bigger crystallites size (Fig.2c and d) was explained by a higher Ti surface density (Table 1).

Concerning textural properties, the distribution of pores diameter was centered near 6.5 nm for the SiO<sub>2</sub>-G support (Figure S2). Both the pores volume and diameter decreased increasing the TiO<sub>2</sub> amount (Table 1, Fig. S2) which revealed that TiO<sub>2</sub> was well deposited into the mesoporous pores which highlighted the interest of this grafting preparation method.

#### 3.2 Characterization of OH groups and acidity

The IR spectra of SiO<sub>2</sub> and TiO<sub>2</sub>/SiO<sub>2</sub> compounds treated at 450 °C under air flow are plotted in Figure S3. Besides the overtones network bands at 1636, 1866 and 1986 cm<sup>-1</sup> of SiO<sub>2</sub> [34], the one observed near 3740 cm<sup>-1</sup> was attributed to stretching vibrations of terminal OH groups which was probably mainly due to silanols [34]. However, stretching vibrations of Ti<sub>v</sub>-μ1-OH entities located on the (001) surface of anatase crystallite could be superimposed in the case of the TiO<sub>2</sub>/SiO<sub>2</sub> compounds [41]. The asymmetric to lower wavenumber of the band at 3740 cm<sup>-1</sup> was due to hydrogen bonding and possibly to the presence of terminal TiOH groups located on other planes than (001) [41]. The diffusion background was too much high for 20.4%TiO<sub>2</sub>/SiO<sub>2</sub>-G leading to poor signal and limiting comparison of the number of OH groups with the bare support.

Acidity of TiO<sub>2</sub>/SiO<sub>2</sub> compounds was characterized in details from FTIR spectra of absorbed CO, acetonitrile, pyridine and NH<sub>3</sub>. IR spectra of CO adsorbed on 20.4%TiO<sub>2</sub>/SiO<sub>2</sub>-G were recorded at 77 K increasing doses after pre-treatment. The evolution plotted in Figure 3 evidenced only one ν(C≡O) band at 2189 cm<sup>-1</sup> for low CO amount which was attributed to β' five-coordinated Ti<sup>4+</sup> sites located on 100 (isostructural with 010) and 101 (isostructural with 011) [42]. Hence, only moderated Lewis acid sites were present on 20.4%TiO<sub>2</sub>/SiO<sub>2</sub>-G. The band shift to 2178 cm<sup>-1</sup> increasing the coverage was explained by the probing of β'' sites and dipole-dipole interactions [42,43]. Additionally, the raise of the band at 2157 cm<sup>-1</sup> associated to a shift of the bands at 3740-3720 cm<sup>-1</sup> to 3650 cm<sup>-1</sup> was attributed to hydrogen bonding of CO with hydroxyl groups [19,20,43]. At high coverage, the band at 2140 cm<sup>-1</sup> was attributed to physisorbed CO. The presence of moderated Lewis sites was confirmed by adsorption of CD<sub>3</sub>CN (Figure S4) through the shift of 41 cm<sup>-1</sup> (2304 cm<sup>-1</sup> instead of 2264 cm<sup>-1</sup> for free molecule) of the ν(C≡N) band [44,45]. The other ν(C≡N) band slightly shifted to 2272 cm<sup>-1</sup> was due to interaction with OH groups [46,47].

The IR spectra of pyridine adsorbed on 20.4%TiO<sub>2</sub>/SiO<sub>2</sub>-G plotted in Figure 4a contained both bands of pyridine coordinated to Lewis sites (1608, 1489 and 1446 cm<sup>-1</sup>) and pyridinium cations formed by reaction of pyridine with Brønsted sites (1640, 1547 and 1489 cm<sup>-1</sup>). The density of Brønsted sites was much smaller than the one of Lewis sites (Figure 1b) so that the compounds could be considered as mostly of Lewis type for this probe. Furthermore, it was null after desorption at 300 °C indicating their strength was weak. The moderated polarizing power of Ti<sup>4+</sup> Lewis sites was shown from the slope of the density value versus the desorption temperature (Figure 4b) and the intermediate shift of the 8a mode of

adsorbed pyridine. Indeed, this latter one was only 25 cm<sup>-1</sup> (from 1583 to 1608 cm<sup>-1</sup>) compared to 44 cm<sup>-1</sup> for strong Lewis sites such as tetrahedral Al<sup>3+</sup> [48,49].

As for pyridine, the spectra of adsorbed NH<sub>3</sub> (Figure 5) revealed the presence of both Lewis ( $\delta_{\text{asym}}(\text{NH}_3)$  band at 1607 cm<sup>-1</sup>) and Brønsted ( $\delta_{\text{asym}}(\text{NH}_4^+)$  band at 1425-1440 cm<sup>-1</sup>) sites [48,50,51]. Using an extinction coefficient value of 8 cm.mol<sup>-1</sup> [51], the density of Brønsted sites probed at 150 °C was ca 15-20? μmol.g<sup>-1</sup> which is much higher than the values obtained for pyridine (4 μmol.g<sup>-1</sup>). It showed that most of the Brønsted sites were weak since NH<sub>3</sub> which is a strong base was able to react with them to form ammonium cations contrarily to pyridine. Anyway, they were much less numerous than the Lewis sites confirming TiO<sub>2</sub>/SiO<sub>2</sub> compounds could be considered as Lewis type. Finally, acidity of bare SiO<sub>2</sub>-G was evaluated under identical experiments (Figure S5). No band of adsorbed NH<sub>3</sub> nor NH<sub>4</sub><sup>+</sup> formed by reaction with Brønsted sites was detected showing the uncovered SiO<sub>2</sub> did not contribute to the overall acidity.

### 3.4 Isobutanol conversion

TiO<sub>2</sub>/SiO<sub>2</sub> catalysts was inactive in the conversion of isobutene at temperature as high as 450 °C. On the opposite, they were active and very selective for the dehydration of isobutanol to butenes from 200 °C. The main product was isobutene but the selectivity value to linear butenes  $S_{\text{LinBut}}$  was significant (ca 30%) which indicated isomerization step took place. Interestingly, very low conversions were measured for blank testing, SiO<sub>2</sub>-G and TiO<sub>2</sub>-P25 (Table 2) which evidenced the presence of specific sites in TiO<sub>2</sub>/SiO<sub>2</sub> catalysts. Selectivity-conversion curves plotted in Figure 6 clearly showed that the selectivity set was almost constant. The  $S_{\text{LinBut}}$  value increased from 29 to 33% at the expense of  $S_{\text{isobut}}$  raising the temperature from 250 to 300 °C (Figure 7). This slight evolution of selectivity was attributed to the temperature dependence of the thermodynamic equilibria between the different butyl carbenium cations leading to butenes [53-56]. An activation energy of 143 kJ.mol<sup>-1</sup> was calculated from the conversions which was higher than the values reported in the literature for alumina, silica-aluminas and silica-beryllium oxide (Table 3). It suggests that weaker active sites were present in the TiO<sub>2</sub>/SiO<sub>2</sub> catalysts. Finally, their slight deactivation with time on stream (Figure S6) cannot be due the very limited structural and textural evolutions observed by XRD (very weak band around 25°, Figure 1) and N<sub>2</sub> isotherms measurements (small decrease in the  $D_{\text{pores}}$  and  $V_{\text{pores}}$  values, Table 1). However, it was explained from TGA/TDA measurements achieved under air flow after 24 h of testing that

revealed weight loss of ca 4% associated with exothermic peaks at 253 and 342 °C (Figure S7) attributed to the presence of soft coke [57-59].

The effect of water on catalytic properties was investigated varying the contact time at 250 °C for feed containing 10% of water or not. Addition of water significantly improved the conversion whereas the  $S_{\text{LinearButenes}}$  value was unchanged (Figure 8). This latter remained also constant with time on stream upon slow deactivation of the catalyst (Figure S6). It suggested that the number of active sites was increased without changing their type and strength which was confirmed by comparison of the apparent activation energies for the two feeds (Table 3). One can notice that if thermodynamic equilibrium was reached, the conversion should decrease adding water to the feed. Finally, the data obtained both at the beginning and at the end of the testing were quite close (Figure 8) which showed both a good reproducibility of measurements and reversibility of the water effect which was explained by *in situ* acidity measurements in the following part.

Commentaire [s11]: voir les vitesses de réaction ()

### 3.3 *In situ* acidity measurements

*In situ* FTIR acidity measurements were preliminary achieved over SiO<sub>2</sub>-G support flowing NH<sub>3</sub> and H<sub>2</sub>O mixtures from room temperature to 450 °C. The spectra plotted in Figure S9 for P<sub>NH<sub>3</sub></sub> 1 kPa and P<sub>H<sub>2</sub>O</sub> 3 kPa contained the bending mode of adsorbed water at 1632-1624 cm<sup>-1</sup> which disappeared above 200 °C and a small  $\delta_{\text{asym}}(\text{NH}_4^+)$  band around 1460 cm<sup>-1</sup> which disappeared above 140 °C. IR observation of NH<sub>4</sub><sup>+</sup> cations could be explained both by the presence of very weak Brønsted sites on the SiO<sub>2</sub> support and by the dissolution of NH<sub>3</sub> in condensed water followed by the spontaneous reaction [60]:



To avoid such contributions, the effect of water on acidity of TiO<sub>2</sub>/SiO<sub>2</sub> catalysts was investigated above 140 °C and more precisely in the reaction temperature range (200-300 °C). *In situ* spectra of 20.4%TiO<sub>2</sub>/SiO<sub>2</sub>-G catalyst recorded at 200 °C flowing 0.2 kPa of NH<sub>3</sub> and different H<sub>2</sub>O partial pressures are plotted in Figure 9. They revealed that the number of Brønsted acid sites (band near 1425 cm<sup>-1</sup>) was strongly increased. The same water effect was observed during the temperature raise and the cooling down (Figure S9) which evidenced that the phenomenon was reversible. At 200 °C, an enhancement factor of 2.5 was determined adding only 0.2% H<sub>2</sub>O and of 4 adding 3% H<sub>2</sub>O. This phenomenon was even stronger at 300 °C since the band at 1425 cm<sup>-1</sup> was quite low under 0.2%NH<sub>3</sub>-He flow and strongly enhanced adding H<sub>2</sub>O (Figure S10). In parallel, the Lewis sites (band at 1606 cm<sup>-1</sup>) remained

unchanged which clearly showed that the improvement of catalytic activity does not arise from conversion of Lewis acid sites into Brønsted acid sites which hence corresponded to water tolerant sites [17-21]. Furthermore, the bending mode of adsorbed H<sub>2</sub>O (band at 1620 cm<sup>-1</sup>) was not observed (Figure 9) indicating the absence of adsorption competition with the NH<sub>3</sub> probe that would hinder the *in situ* acidity measurements.

The evolution of OH groups under the different flows was limited to TiO<sub>2</sub>/SiO<sub>2</sub>-A compounds because of strong diffusion background at high wavenumbers for the TiO<sub>2</sub>/SiO<sub>2</sub>-G series (Figure S3). The IR spectrum of 19.5%TiO<sub>2</sub>/SiO<sub>2</sub>-A recorded at 250 °C under 3% H<sub>2</sub>O-He flow and plotted in Figure 10 revealed the presence of adsorbed water (bending mode at 1604 cm<sup>-1</sup> and stretching broad band around 3500 cm<sup>-1</sup>) [61,62] interacting by hydrogen bonds with terminal OH groups (negative band at 3742 cm<sup>-1</sup>) or by coulombic interaction with Lewis sites. Furthermore, an additional band appeared at 3664 cm<sup>-1</sup> whose attribution was hard from the literature data since it could correspond either to bridging OH groups [62,63] or to hydrogen bonded OH groups [62,63b] or to Ti<sub>VI</sub>-OH<sub>2</sub> located on the (101) surface of anatase crystallites [41].

Under 1% NH<sub>3</sub>-He, the negative band at 3742 cm<sup>-1</sup> indicated H-bonding of terminal OH with NH<sub>3</sub>. Furthermore, the observation of  $\nu_{as}(\text{NH}_3)$ ,  $\nu_s(\text{NH}_3)$  and  $\delta(\text{NH}_3)$  bands at 3378-3336, 3251 and 1604 cm<sup>-1</sup> respectively revealed that NH<sub>3</sub> was mainly bonded to Lewis sites as well as interacting with OH groups [49,64,65]. The weak band at 1424 cm<sup>-1</sup> was attributed to  $\delta_{asym}(\text{NH}_4^+)$  due to weak Brønsted acidity in agreement with the data obtained for 20.4%TiO<sub>2</sub>/SiO<sub>2</sub>-G (Figure 5). Note that similar Brønsted to Lewis bands ratios were obtained for 19.5%TiO<sub>2</sub>/SiO<sub>2</sub>-A and 20.4%TiO<sub>2</sub>/SiO<sub>2</sub>-G. Finally, the negative band at 3708 cm<sup>-1</sup> was assigned to acidic OH groups leading to NH<sub>4</sub><sup>+</sup> formation and the one at 3162 cm<sup>-1</sup> was assigned to  $\nu_{asym}(\text{NH}_4^+)$  stretching vibrations [66].

Finally, under 3% H<sub>2</sub>O+1% NH<sub>3</sub> flow, the strong enhancement of the band at 1424 cm<sup>-1</sup> was associated to a strong decrease of the band at 3664 cm<sup>-1</sup> (and to a lesser extent of the one at 3708 cm<sup>-1</sup>) and revealed that NH<sub>4</sub><sup>+</sup> groups were formed by reaction of NH<sub>3</sub> and H<sup>+</sup> arising from the corresponding OH groups formed under water vapor.

#### 4. Discussion

Titania-silica materials have been extensively used as catalysts and supports for a wide variety of reactions since the interaction of TiO<sub>2</sub> with SiO<sub>2</sub> generates new catalytic active sites [67]. In this work, TiO<sub>2</sub>/SiO<sub>2</sub> compounds prepared by a grafting method were shown to

be much more active in the dehydration of isobutanol than the corresponding simple oxides. These catalysts contained mainly TiO<sub>2</sub> amorphous clusters and few TiO<sub>2</sub> nanocrystallites bridged with the SiO<sub>2</sub> via Ti-O-Si bonds. Such bonds were formed during the Ti grafting step and their existence was suggested by the shift of the Ti 2p<sub>3/2</sub> XPS band.

The acidic properties of TiO<sub>2</sub>/SiO<sub>2</sub> compounds were quite different from TiO<sub>2</sub> since they owned both moderated Lewis and weak Brønsted acidity whereas strong and moderated Lewis sites are present in bulk titania [20,62,64,68-70]. As TiO<sub>2</sub>-P25 was much less active in the dehydration of isobutanol than TiO<sub>2</sub>/SiO<sub>2</sub> catalysts, it showed that if Lewis sites were active, their contribution was much smaller than the weak Brønsted sites that were associated to Ti-O-Si bonds [67]. Considering the Tanabe [71] and Dumesic [70] models, the Brønsted acidity of Ti-O-Si bonds is generated by a charge unbalance between tetrahedral Si<sup>4+</sup> and octahedral or pentahedral Ti<sup>4+</sup> cations. Note that tetrahedral Ti<sup>4+</sup> cations unable to generate Brønsted acidity [67] were not present in the TiO<sub>2</sub> clusters anchored on the SiO<sub>2</sub> supports (no strong Lewis sites).

As TiO<sub>2</sub>/SiO<sub>2</sub> catalysts were inactive for isomerization of isobutene and as their selectivity of linear butenes was almost constant with the contact time in the conversion of isobutanol and was close to values reported in the literature (31-33%) for different catalysts, it was concluded that the linear butenes were not formed by successive isomerization of isobutene but thermodynamic equilibrium between the four carbocations [53]. Hence, the acid sites located at the Ti-O-Si bonds did not participate to the isomerization step.

Additionally, the water effects on TiO<sub>2</sub>/SiO<sub>2</sub> acidic catalysts were investigated for the dehydration of isobutanol. Water was produced by the reaction itself and added or not to the reaction feed. While only very limited structural and textural evolutions were observed after 29 h on stream, a significant increase in the catalytic activity was evidenced adding water. The use of *in situ* acidity measurements achieved under flows containing water vapor at the reaction temperatures has shown that the density of Brønsted acid sites increased in the presence of water while the Lewis sites remained unchanged. Hence, this latter ones seemed to be unable to dissociate water because not strong enough whereas the increase in Brønsted acidity under water vapor was related to formation of acidic OH groups by hydrolysis of Ti-O-Si bonds. Even if hydrolysis of bridging bonds is more favorable for tetrahedral cations, only pentahedral and octahedral Ti cations are able to generate Brønsted acidity. Furthermore, the location at 3664 cm<sup>-1</sup> of the ν(O-H) vibrations corresponded to bridging OH groups. Considering the absence of Lewis to Brønsted conversion, pseudo bridging OH groups interacting cations were assumed to be formed under water vapor according to the scheme

Commentaire [s12]: voir refs biblio

Commentaire [s13]: voir biblio

plotted in Figure 11. These Brønsted sites reacted with  $\text{NH}_3$  to form  $\text{NH}_4^+$  cations observed under water containing flows at the reaction temperatures and corresponded to the active sites leading to activity enhancement in the dehydration of isobutanol.

## 5. Conclusions

In this work, the water effects on  $\text{TiO}_2/\text{SiO}_2$  acid catalysts used for the gas phase conversion of isobutanol into linear olefins have been investigated. Such compounds synthesized by grafting corresponded to  $\text{TiO}_2$  amorphous clusters over mesoporous  $\text{SiO}_2$  containing after activation at  $450^\circ\text{C}$  under dry oxygen mostly moderated Lewis and few weak Brønsted acid sites. They were shown to be much more active than separated  $\text{TiO}_2$  and  $\text{SiO}_2$  and provided only dehydration products among which 30% of linear butenes.

Furthermore, the catalytic activity was significantly enhanced by addition of water into the feed whereas the selectivity to linear butenes was unchanged. This phenomenon was not due to any change in the structural or textural properties of the solid. Activation energy measurements indicated that the nature and strength of active sites was similar. *In situ* FTIR acidity measurements achieved flowing  $\text{NH}_3$  and  $\text{H}_2\text{O}$  at the reaction temperatures have showed that the amount of Lewis sites remained constant under water vapor. However, a large increase in the density of Brønsted acid sites was evidenced which explained the activity improvement. Hence, in spite of a limited number after activation at  $450^\circ\text{C}$ , the weak Brønsted acid sites of  $\text{TiO}_2/\text{SiO}_2$  catalysts appeared as the active sites contrarily to the Lewis ones. They could be partly generated by the dehydration reaction itself and furthermore, adding water to the feed. Hydrolysis of Ti-O-Si bonds specifically present in  $\text{TiO}_2/\text{SiO}_2$  compounds would generate OH pseudo bridging groups at the origin of Brønsted acidity.

Finally, the methodology used in this work to unravel the water effects on acid catalysts can be transposed to others catalysts and reactions. In particular, *in situ* acidity measurements achieved under water vapor appeared as very powerful and should be generalized.

## Acknowledgments

This work has been cofounded by INC/CNRS (Z. Buniazet PhD thesis grant) and IFPEN. Luis Cardenas is warmly acknowledged for fruitful discussion and quick complementary XPS experiments.



## References

- [1] F. Obenaus, W. Droste, J. Neumeister, in W. Gerhartz, Y. Yamamoto, F.T. St. Campbell, R. Pfefferkorn, J.F. Rounsaville (Eds.) *Ullmann's Encyclopedia of Industrial chemistry*, 5th ed., Vol. A4, VCH, Weinheim, 1985-1986, p. 483.
- [2] P. Dürre, *Curr. Opin. Biotechnol.* 22 (2011) 331–336.
- [3] Y. Ni, Z.H. Sun, *Appl. Microbiol. Biotechnol.* 83 (2009) 415-423.
- [4] N. Qureshi, T.C. Ezeji, *Biofuels, Bioprod. Biorefin.* 2 (2008) 319-330.
- [5] S. Atsumi, T. Hanai, J.C. Liao, *Nature* 451 (2008) 86-90.
- [6] M. Mascal, *Biofuels Bioprod. Bioref.* 6 (2012) 483–493.
- [7] C.D. Baertsch, K.T. Komala, Y.H. Chua, E. Iglesia, *J. Catal.* 205 (2002) 44-57.
- [8] C. Adam, D. Minoux, N. Nesterenko, S. Van Donk, J.-P. Dath, WO 2011113834 (2011), to Total Petrochemicals.
- [9] A. Chaumonnot, V. Coupard, S. Maury, FR 2988717 (2013), to IFP Energies Nouvelles.
- [10] V. Macho, M. Kralik, E. Jurecekova, J. Hudec, L. Jurecek, *Appl. Catal. A: Gen.* 214 (2001) 251-257.
- [11] A. Corma, M. Renz, *Chem. Commun.* (2004) 550-551.
- [12] M.W. Hahn, J.R. Copeland, A.H. van Pelt, C. Sievers, *ChemSusChem*, 6 (2013) 2304-2315.
- [13] L. Li, Y. Yoshinaga, T. Okuhara, *Phys. Chem. Chem. Phys.* 4 (2002) 6129-6136.
- [14] R.M. West, D.J. Braden, J.A. Dumesic, *J. Catal.* 262 (2009) 134-143.
- [15] D. Zhang, S. A.I. Barri, D. Chadwick, *Appl. Catal. A: Gen.* 403 (2011) 1-11.
- [16] D. Zhang, R. Al-Hajri, S.A.I. Barri, D. Chadwick, *Chem. Commun.* 46 (2010) 4088-4090.
- [17] K. Nakajima, Y. Baba, R. Noma, M. Kitano, J.N. Kondo, S. Hayashi, M. Hara, *J. Am. Chem. Soc.* 133 (2011) 4224-4227.
- [18] R.M. West, D.J. Braden, J.A. Dumesic, *J. Catal.* 262 (2009) 134-143.
- [19] H. Shintaku, K. Nakajima, M. Kitano, N. Ichikuni, M. Hara, *ACS Catal.* 4 (2014) 1198-1204.
- [20] K. Nakajima, R. Noma, M. Kitano, M. Hara, *J. Phys. Chem. C* 117 (2013) 16028-16033.
- [21] Y. Wang, F. Wang, Q. Song, Q. Xin, S. Xu, J. Xu, *J. Am. Chem. Soc.* 135 (2013) 1506-1515.
- [22] T. Yamaguchi, K. Tanabe, *Bull. Chem. Soc. Jap.* 47(2) (1974) 424-429.

- [23] J.H. Kwak, D. Mei, C.H.F. Peden, R. Rousseau, J. Szanyi, *Catal. Lett.* 141 (2011) 649-655.
- [24] F. Berube, B. Nohair, F. Kleitz, S. Kaliaguine, *Chem. Mater.* 2010, 22, 1988-2000.
- [25] I.S. Pieta, M. Ishaq, R.P.K. Wells, J.A. Anderson, *Appl. Catal. A: Gen.* 390 (2010) 127-134.
- [26] M. Tamura, K. Shimizu, A. Satsuma, *Appl. Catal. A: Gen.* 433-434 (2012) 135-145.
- [27] C.A. Emeis, *J. Catal.* 141 (1993) 347-354.
- [28] T. Chafik, O. Dulaurent, J.L. Gass, D. Bianchi, *J. Catal.* 179 (1998) 503-514.
- [29] F. Giraud, J. Couble, C. Geantet, N. Guilhaume, E. Puzenat, S. Gros, L. Porcheron, M. Kanniche, D. Bianchi, *J. Phys. Chem.C*, 119 (2015) 16089-16105.
- [30] S.-Y. Chen, T. Mochizuki, Y. Abe, M. Toba, Y. Yoshimura, *Appl. Catal. B: Environm.* 148-149 (2014) 344-356.
- [31] T.R. Eaton, M.P. Campos, K.A. Gray, J.M. Notestein, *J. Catal.* 309 (2014) 156-165.
- [32] T. Ohsaka, F. Izumi, Y. Fujiki, *J. Raman. Spectrosc.* 7(6) (1978) 321-324.
- [33] M.-S. Zhang, Z. Yin, Q. Chen, *Ferroelectrics* 168 (1995) 131-137.
- [34] H. Launay, S. Loridant, A. Pigamo, J.-L. Dubois, J.M.M. Millet, *J. Catal.* 246 (2007) 390-398.
- [35] S. Sahoo, A.K. Arora, V. Sridharan, *J. Phys. Chem. C* 113 (2009) 16927-16933.
- [36] Y. Lei, L.D. Zhang, J.C. Fan, *Chem. Phys. Lett.* 338 (2001) 231-236.
- [37] K.-R. Zhu, M.-S. Zhang, Q. Chen, Z. Yin, *Phys. Lett. A* 340 (2005) 220-227.
- [38] V. Swamy, A. Kuznetsov, L.S. Dubrovinsky, R.A. Caruso, D.G. Shchukin, B.C. Muddle, *Phys. Rev. B* 71 (2005) 184302.
- [39] F. Bérubé, B. Nohair, F. Kleitz, S. Kaliaguine, *Chem. Mater.* 22 (2010) 1988-2000.
- [40] U. Sirimahachai, N. Ndiege, R. Chandrasekharan, S. Wongnawa, M.A. Shannon, *Sol-Gel Sci. Technol.* 60 (2010) 56-53.
- [41] C. Arrouvel, M. Digne, M. Breyse, H. Toulhoat, P. Raybaud, *J. Catal.* 222 (2004) 152-166.
- [42] K. Hadjiivanov, J. Lamotte, J.-C. Lavalley, *Langmuir* 13 (1997) 3374-3381.
- [43] M. Kitano, E. Wada, K. Nakajima, S. Hayashi, S. Miyazaki, H. Kobayashi, M. Hara, *Chem. Mater.* 25 (2013) 385-393.
- [44] E. Gianotti, L. Marchese, M. Guidotti, N. Ravasio, R. Psaro, S. Coluccia, *Stud. Surf. Sci. Catal.* 155 (2005) 311-320.
- [45] F. Bonino, A. Damin, S. Bordiga, C. Lamberti, A. Zecchina, *Langmuir*, 19 (2003) 2155-2161.

- [46] J. Chen, J. Meurig Thomas, G. Sankar, *J. Chem. Soc. Faraday Trans* 90 (1994) 3455-3459.
- [47] C.L. Angel, M.V. Howell, *J. Phys. Chem.* 73, (1969) 2551-?.
- [48] G. Busca, *Phys. Chem. Chem. Phys.* 1 (1999) 723-736.
- [49] G. Busca, *Catal. Today* 41 (1998) 191-206.
- [50] F. Giraud, C. Geantet, N. Guilhaume, S. Loridant, S. Gros, L. Porcheron, M. Kanniche, D. Bianchi, *J. Phys. Chem. C* 118 (2014) 15677–15692.
- [51] A. Zecchina, L. Marchese, S. Bordiga, C. Pazè, E. Gianotti, *J. Phys. Chem. B* 101 (1997) 10128-10135.
- [52] A. Vimont, J.-C. Lavalley, L. Francke, A. Demourgues, A. Tressaud, M. Daturi, *J. Phys. Chem. B* 108 (2004) 3246-3255.
- [53] N.S. Kotsarenko, L.V. Malysheva, *Kinetika i Kataliz* 24 (1983) 743-748.
- [54] V. Macho, M. Králik, E. Jurecekova, J. Hudecd, L. Jurecek, *Appl. Catal. A: Gen.* 214 (2001) 251–257.
- [55] A.G. Stepanov, K.I. Zamaraev, *Catal. Lett.* 19 (1993) 153-158.
- [56] J.D. Taylor, M. Jenni, M.W. Peters, *Top. Catal.* 53 (2010) 1224-1230.
- [57] H. Zhang, S. Shao, R. Xiao, D. Shen, J. Zeng, *Energ. Fuel.*, 28 (2014) 52-57.
- [58] I. V. Kozhevnikov, S. Holmes, M.R.H. Siddiqui, *Appl. Catal. A: Gen.* 214 (2001) 47-58.]
- [59] A.R. Pradhan, J.F. Wu, S.J. Jong, T.C. Tsai, S.B. Liu, *Appl. Catal. A: Gen.* 165 (1997) 489-497.
- [60] W. Lang, T.M. Blöck, R. Zander, *Clin. Chim. Acta* 273 (1998) 43–58.
- [61] C. Morterra, *J. Chem. Soc., Faraday Trans. I* 84 (1988) 1617-1637.
- [62] G. Martra, *Appl. Catal. A: Gen.* 200 (2000) 275–285.
- [63] A.A. Tsyganenko, V.N. Filimonov, *J. Mol. Structure* 19 (1973) 579-589.
- [63b] Z. Liu, J. Tabora, R. J. Davis, *J. Catal.* 149 (194) 117-126.
- [64] G. Ramis, G. Busca, F. Bregani, P. Forzatti, *Appl. Catal.* 64 (1990) 243-257.
- [65] G. Ramis, G. Busca, F. Bregani, P. Forzatti, *Appl. Catal.* 64 (1990) 259-277.
- [66] J. P. Mathieu H. Poulet, *Spectrochim. Acta* 16 (1980) 696-703.
- [67] X. Gao, I. E. Wachs, *Catal.Today* 51 (1999) 233-254.
- [68] R. J. Davis, Z. Liu, *Chem. Mater.* 9 (1997) 2311-2324.
- [69] F. Giraud, C. Geantet, N. Guilhaume, S. Gros, L. Porcheron, M. Kanniche, D. Bianchi, *J. Phys. Chem. C* 118 (2014) 15664-15676.
- [70] T. Kataoka, J.A. Dumesic, *J. Catal.* 112 (1988) 66-79.

[71] K. Tanabe, T. Sumiyoshi, K. Shibata, T. Kiyoura, J. Kitagawa, Bull. Chem. Soc. Jpn. 47 (1974) 1064-1066.

**Table 1.** Chemical compositions and textural parameters of TiO<sub>2</sub>/SiO<sub>2</sub> compounds and of the corresponding supports.

Compound	Theo. Ti weight %	ICP Ti weight %	Ti/Si (mol/mol)	Surface density (at Ti.nm <sup>2</sup> )	S <sub>BET</sub> (m <sup>2</sup> .g <sup>-1</sup> )	D <sub>pores</sub> (nm)	V <sub>pores</sub> (cm <sup>3</sup> .g <sup>-1</sup> )
SiO <sub>2</sub> -G	0	-	-	-	557	6.5	0.85
14.2%TiO <sub>2</sub> /SiO <sub>2</sub> -G	10.7	8.5	0.12	3.2	387	5.4	0.62
18.7%TiO <sub>2</sub> /SiO <sub>2</sub> -G	12.2	11.2	0.17	4.5	385	4.9	0.53
20.4%TiO <sub>2</sub> /SiO <sub>2</sub> -G	13.5	12.2	0.19	5.0	381	4.8	0.52
20.4%TiO <sub>2</sub> /SiO <sub>2</sub> -G used	13.5	12.2	0.19	5.0	403	4.1	0.43
SiO <sub>2</sub> -A	0	-	-	-	215	16.1	0.68
11.8%TiO <sub>2</sub> /SiO <sub>2</sub> -A	7.1	7.1	0.10	5.5	186	11.2	0.44
19.5%TiO <sub>2</sub> /SiO <sub>2</sub> -A	12.5	11.7	0.18	9.7	189	12.8	0.50

**Table 2.** Comparison of catalytic properties of SiO<sub>2</sub>, TiO<sub>2</sub>/SiO<sub>2</sub> and TiO<sub>2</sub>. Feed composition (iC<sub>4</sub>OH/inert 30/70), Temperature 275 °C, 1/WHSV 7-8 h.g.mol<sup>-1</sup> except for TiO<sub>2</sub>-P25: 17 h.g.mol<sup>-1</sup>.

Catalyst	Conversion (%)	Reaction rate (μmol.s <sup>-1</sup> .g <sup>-1</sup> )	S <sub>isobutene</sub> (%)	S <sub>1-butene</sub> (%)	S <sub>trans 2-butene</sub> (%)	S <sub>cis 2-butene</sub> (%)
Empty reactor	< 2 %	<0.0?	-	-	-	-
SiO <sub>2</sub> -G	< 2 %	<0.0?	-	-	-	-
20.4%TiO <sub>2</sub> / SiO <sub>2</sub> -G	38	??	69	10	10	11
19.5 %TiO <sub>2</sub> / SiO <sub>2</sub> -A	37	??	71	9	10	10
TiO <sub>2</sub> -P25	2	0.0?	78	8	7	7

**Table 3.** Activation energy values in the catalytic dehydration of isobutanol.

Catalyst	T ( °C)	Feed composition (iC <sub>4</sub> OH/H <sub>2</sub> O/inert)	Ea (kJ.mol <sup>-1</sup> )	Reference
20.4%TiO <sub>2</sub> /SiO <sub>2</sub> -G	250-300	35/0/65	143	This study
20.4%TiO <sub>2</sub> / SiO <sub>2</sub> -G	250-300	36/14/50	147	This study
94.3%SiO <sub>2</sub> -5.7%Al <sub>2</sub> O <sub>3</sub>	275-300	3/0/97	100	[53]
97.2%SiO <sub>2</sub> -2.8%Al <sub>2</sub> O <sub>3</sub>	275-300	3/0/97	92	[53]
62.5%SiO <sub>2</sub> -37.5%BeO	275-300	3/0/97	88	[53]
γ-Al <sub>2</sub> O <sub>3</sub>	275-300	3/0/97	117	[53]

## FIGURES CAPTIONS

**Figure 1:** XRD patterns of TiO<sub>2</sub>/SiO<sub>2</sub> catalysts.

**Figure 2:** TEM images of (a,b) 20.4%TiO<sub>2</sub>/SiO<sub>2</sub>-G and (c,d) 19.5%TiO<sub>2</sub>/SiO<sub>2</sub>-A catalysts. Red curves were added around TiO<sub>2</sub> nanoparticles for easier visualization.

**Figure 3:** Evolution of IR spectra of 20.4%TiO<sub>2</sub>/SiO<sub>2</sub> catalysts recorded after pretreatment, adsorption of different doses of CO at 77 K and evacuation. The background corresponded to the spectrum recorded under dry air flow after pretreatment, mass of the pellet 25 mg.

**Figure 4:** Evolution of IR spectra of 20.4%TiO<sub>2</sub>/SiO<sub>2</sub> catalysts recorded after pretreatment, adsorption of pyridine at RT and evacuation at increasing temperature. The backgrounds corresponded to the spectra recorded under dry air flow after pretreatment, mass of the pellet 19 mg.

**Figure 5:** Evolution of IR spectra of 20.4%TiO<sub>2</sub>/SiO<sub>2</sub>-G catalysts recorded after pretreatment under 0.2%NH<sub>3</sub>-He flow at different temperatures. The backgrounds corresponded to the spectra recorded under He flow after pretreatment, mass of the pellet 24 mg.

**Figure 6:** Conversion-Selectivity curves obtained for 20.4%TiO<sub>2</sub>/SiO<sub>2</sub>-G catalyst. Feed composition iC<sub>4</sub>OH/N<sub>2</sub> 30/70, 1/WHSV 7.7-21.7 h.g.mol<sup>-1</sup>, temperature 250 °C.

**Figure 7:** Evolution of conversion and S<sub>LinrBut</sub> value with the reaction temperature. Feed composition iC<sub>4</sub>OH/N<sub>2</sub> : 35/65, 1/WHSV 7.5 h.g.mol<sup>-1</sup>.

**Figure 8:** Evolution of conversion and S<sub>LinrBut</sub> value with the 1/WHSV parameter. Feed composition: iC<sub>4</sub>OH/inert: 31/69 (black curves) iC<sub>4</sub>OH/H<sub>2</sub>O/inert: 31/10/59 (red curves), Temperature 250 °C. The up and down triangles correspond to the conversions and S<sub>LinBut</sub> values respectively measured at the end of the catalytic testings for the two feeds.

**Figure 9:** Evolution with the H<sub>2</sub>O partial pressure of the IR spectra of 20.4%TiO<sub>2</sub>/SiO<sub>2</sub>-G recorded under different NH<sub>3</sub>/H<sub>2</sub>O/He flows at 200 °C. The background corresponded to the spectrum recorded under He flow at 200 °C, mass of the pellet 30 mg.

**Figure 10:** IR spectra of 19.5%TiO<sub>2</sub>/SiO<sub>2</sub>-A recorded under 3% H<sub>2</sub>O, 1% NH<sub>3</sub>, 3% H<sub>2</sub>O+1% NH<sub>3</sub> at 250 °C. The background corresponded to the spectrum recorded under He flow at 250 °C, mass of the pellet 14 mg.

**Figure 11:** Hydrolysis scheme of Ti-O-Si bonds located at the interface between TiO<sub>2</sub> amorphous clusters and SiO<sub>2</sub> support. The pseudo bridging OH bonds corresponded to Brønsted acid sites leading to activity enhancement by addition of water vapor to the feed.

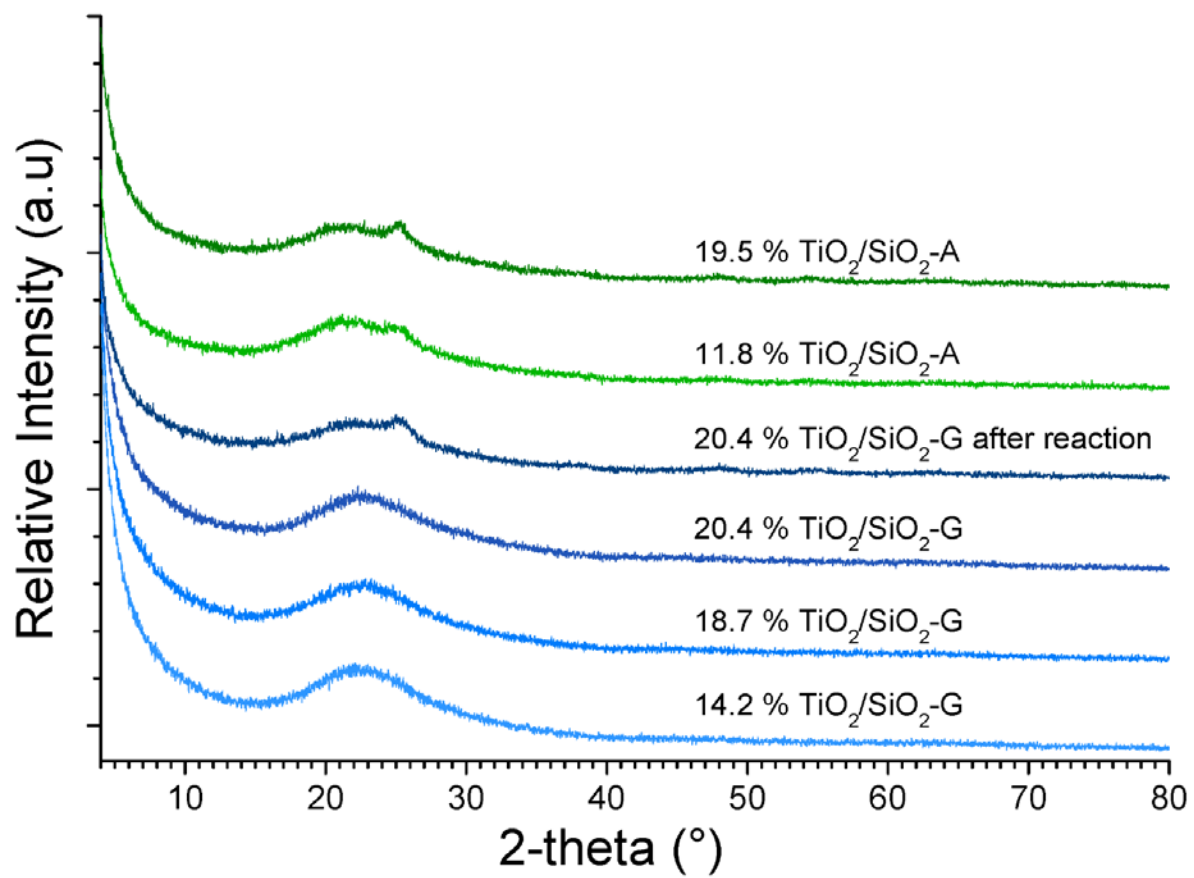


**Figure 1:** XRD patterns of TiO<sub>2</sub>/SiO<sub>2</sub> compounds.

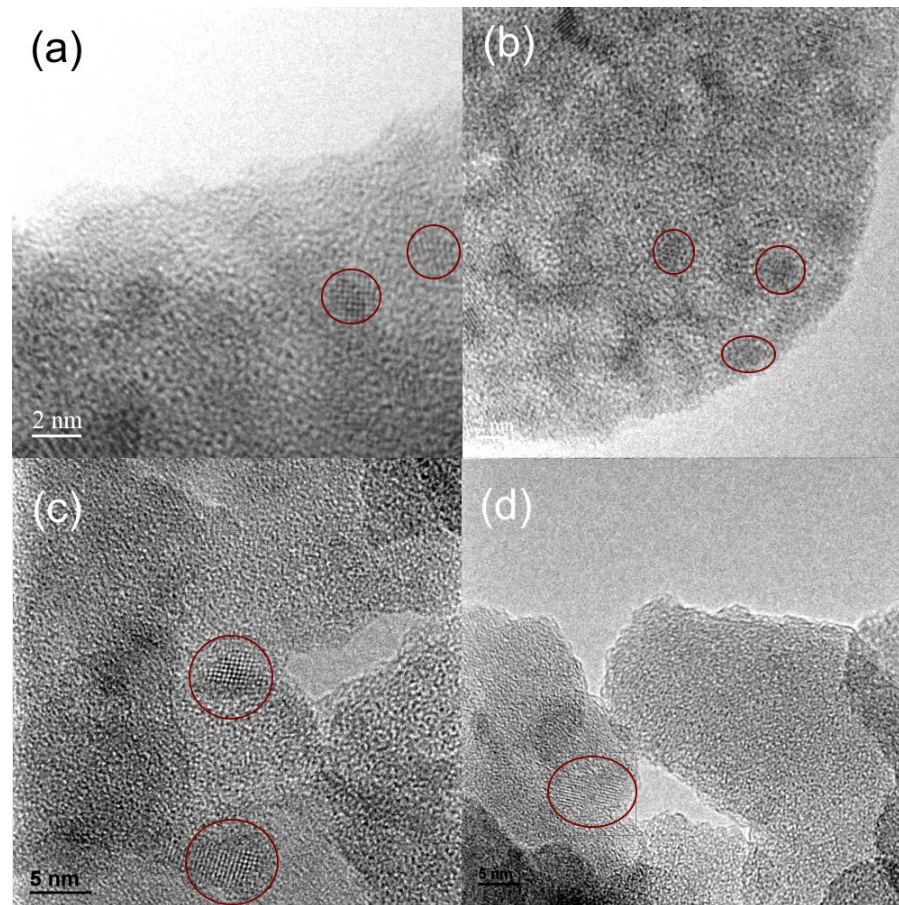


**Figure 2:** TEM images of (a,b) 20.4%TiO<sub>2</sub>/SiO<sub>2</sub>-G and (c,d) 19.5%TiO<sub>2</sub>/SiO<sub>2</sub>-A catalysts. For easier visualization, red curves were added around few TiO<sub>2</sub> nanocrystallites present among amorphous TiO<sub>2</sub> clusters.

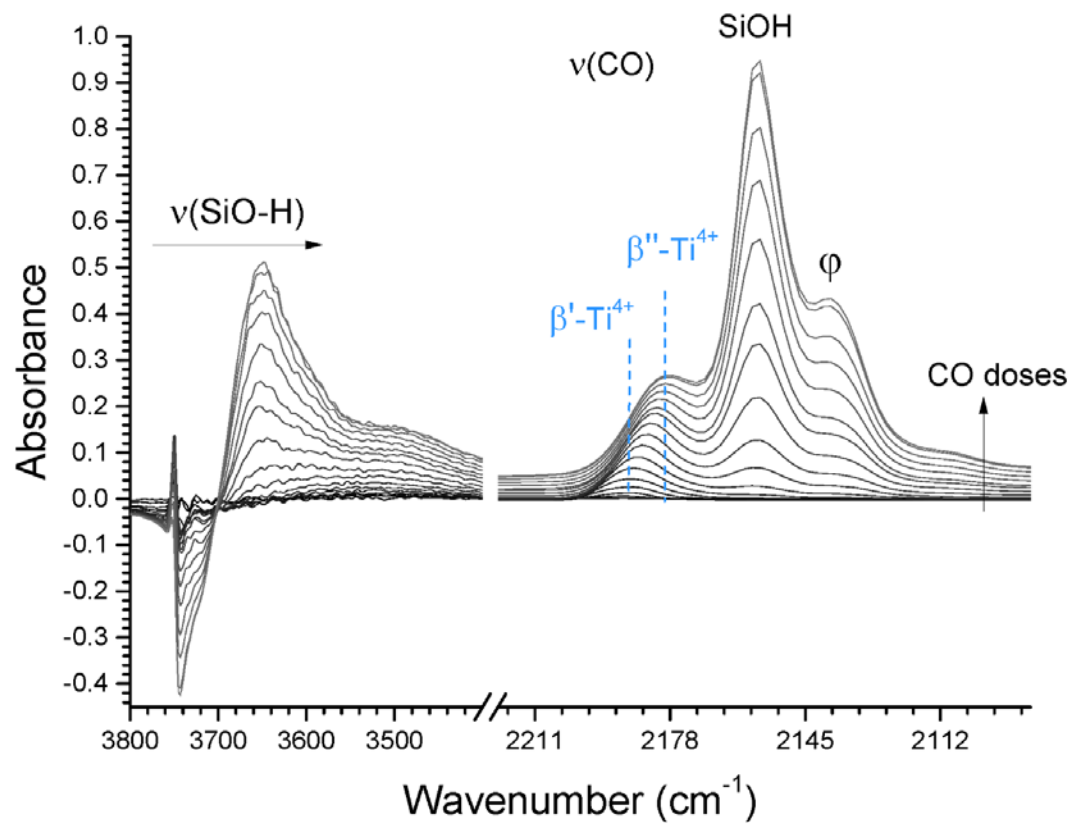


**Figure 3:** Evolution of IR spectrum of 20.4%TiO<sub>2</sub>/SiO<sub>2</sub> catalyst recorded after pretreatment, adsorption of different doses of CO at 77 K and evacuation. The background corresponded to the spectrum recorded at 77 K after pretreatment, mass of the pellet 25 mg.

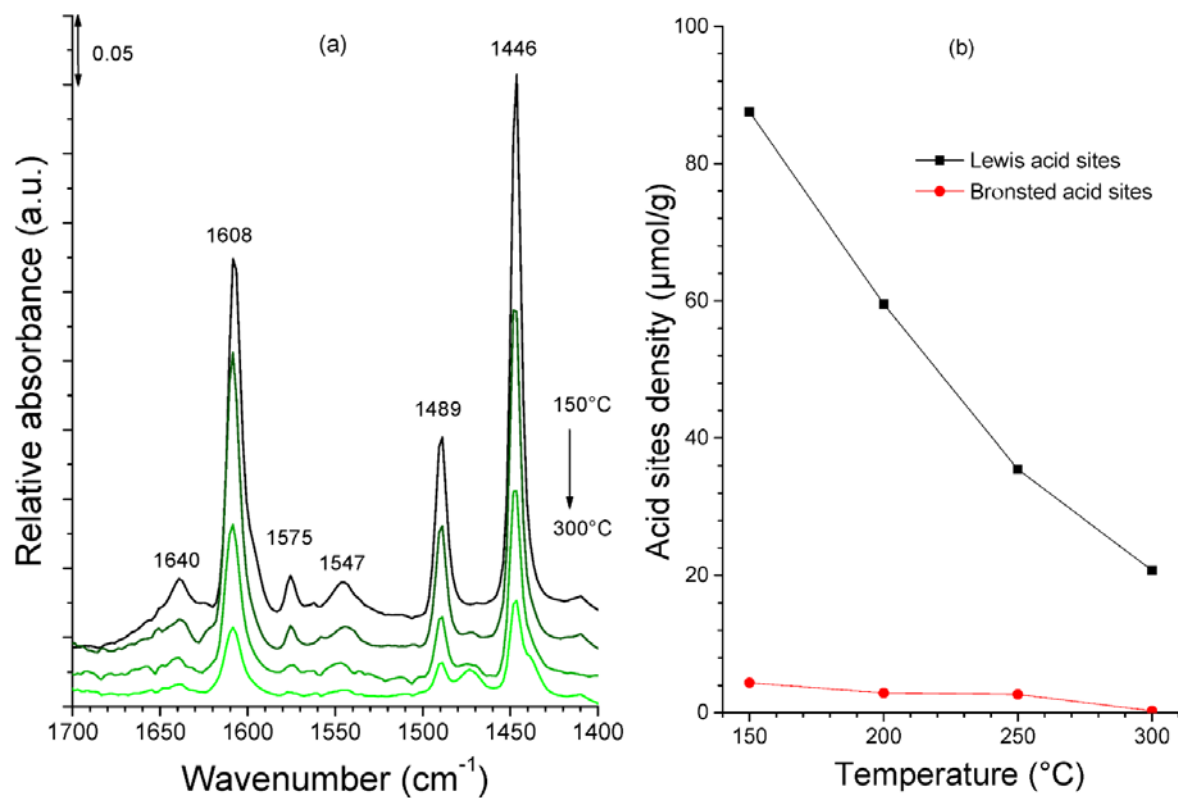


**Figure 4:** Evolution of IR spectrum of 20.4%TiO<sub>2</sub>/SiO<sub>2</sub> catalyst recorded after pretreatment, adsorption of pyridine at RT and evacuation at increasing temperature. The background corresponded to the spectrum recorded at RT under dry air flow after pretreatment, mass of the pellet 19 mg.

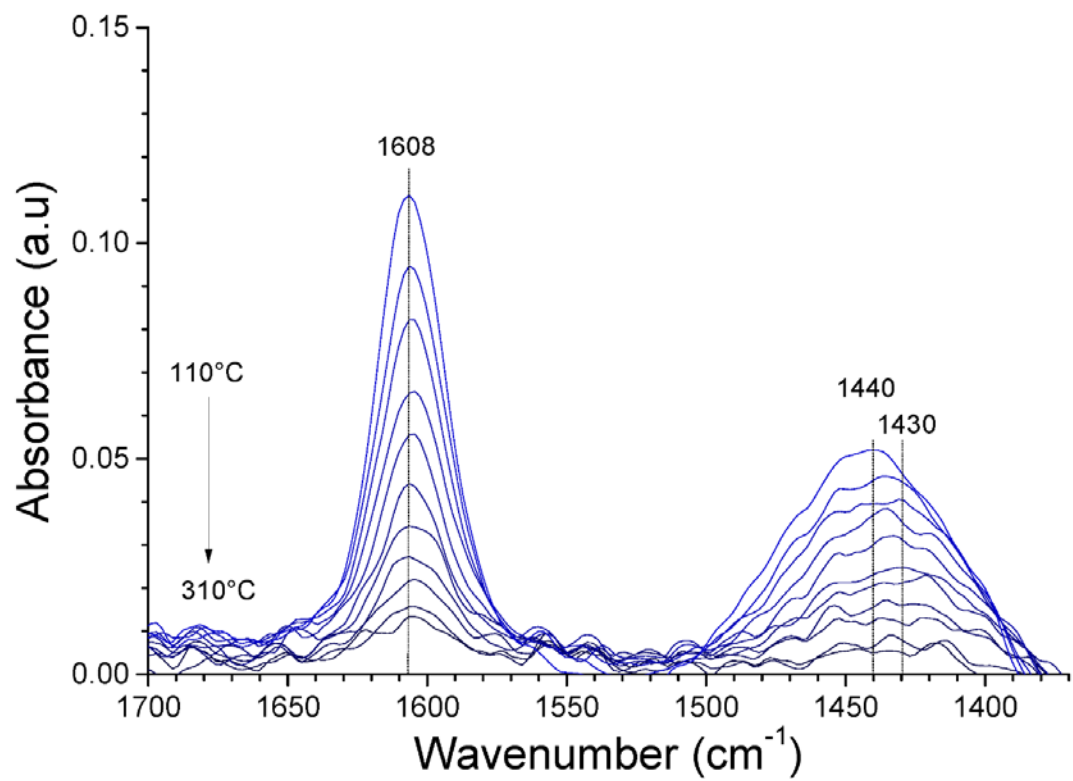


**Figure 5:** Evolution of IR spectrum of 20.4%TiO<sub>2</sub>/SiO<sub>2</sub>-G catalyst recorded under 0.2%NH<sub>3</sub>-He flow at different temperatures after pretreatment. The backgrounds corresponded to the spectra recorded under He flow at the same temperatures after pretreatment, mass of the pellet 24 mg.

**Figure 6:** Conversion-Selectivity curves obtained for 20.4%TiO<sub>2</sub>/SiO<sub>2</sub>-G catalyst. Feed composition iC<sub>4</sub>OH/N<sub>2</sub> 31/69, 1/WHSV 7.7-21.7 h.g.mol<sup>-1</sup>, temperature 250 °C.

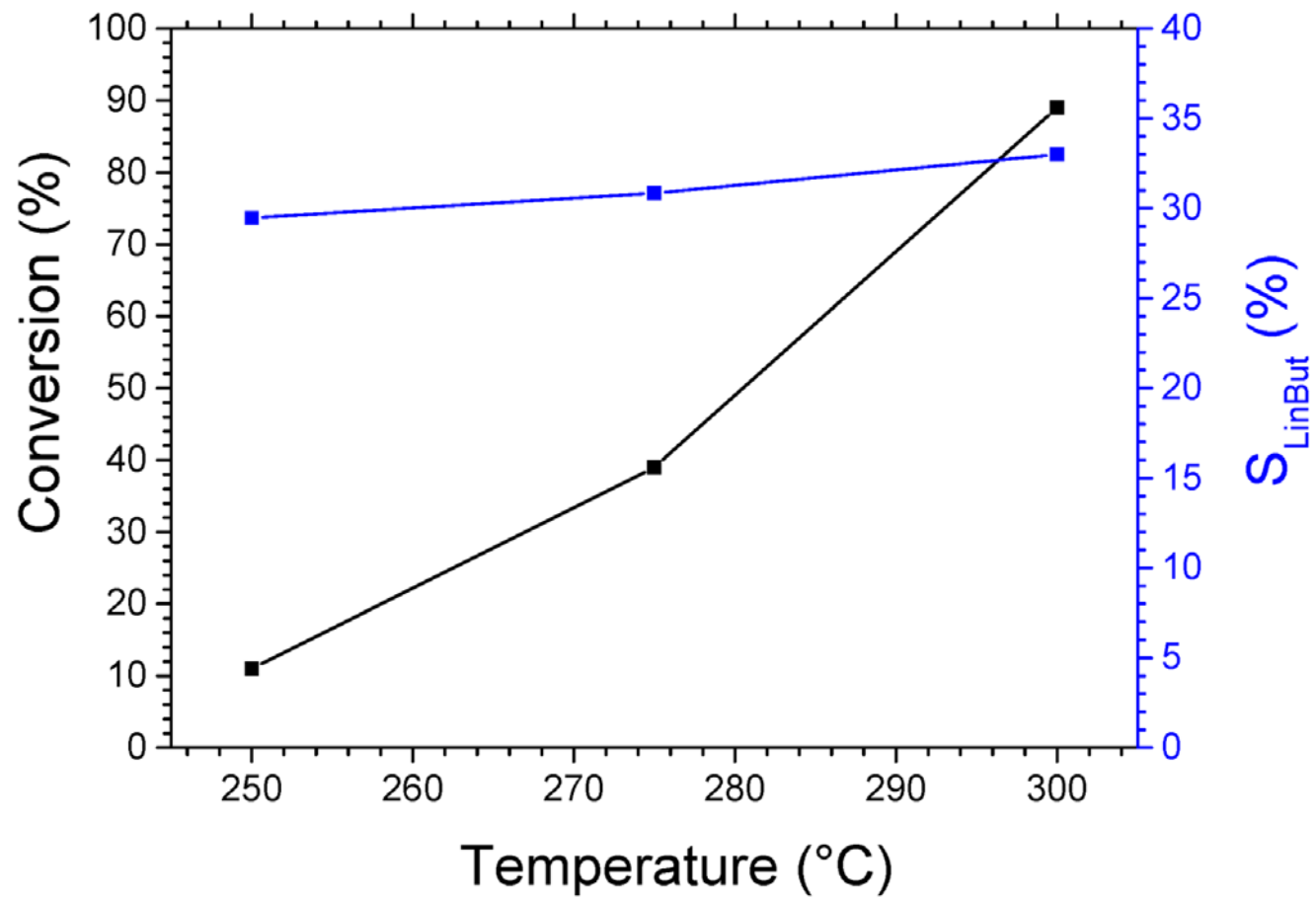


**Figure 7:** Evolution of the conversion and  $S_{LinBut}$  values with the reaction temperature. Feed composition  $iC_4OH/N_2$  : 35/65, 1/WHSV 7.5  $h.g.mol^{-1}$ .

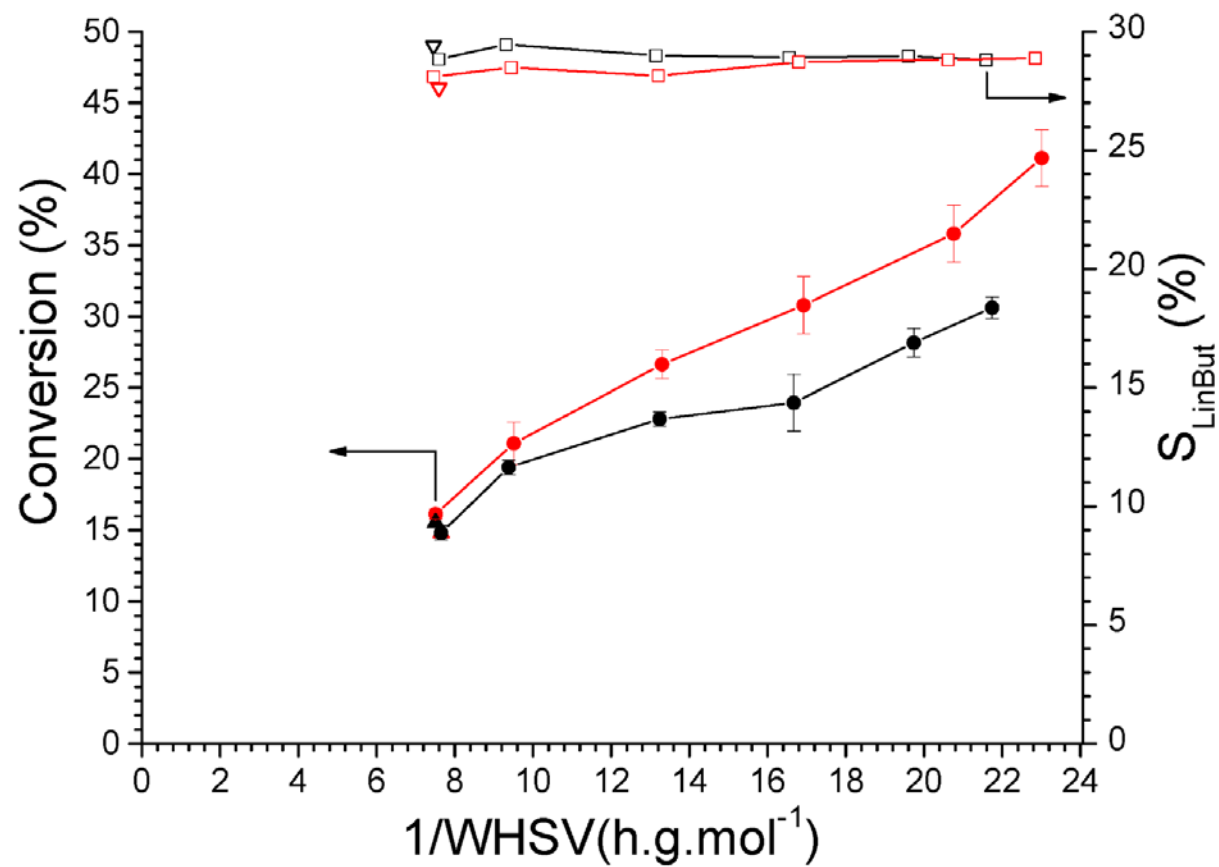


**Figure 8:** Evolution of the conversion and  $S_{\text{LinBut}}$  values with the  $1/\text{WHSV}$  parameter. Feed composition:  $i\text{C}_4\text{OH}/\text{inert}$ : 31/69 (black curves)  $i\text{C}_4\text{OH}/\text{H}_2\text{O}/\text{inert}$ : 31/10/59 (red curves), Temperature 250 °C. The up and down triangles correspond to the conversions and  $S_{\text{LinBut}}$  values respectively measured at the end of the catalytic testings for the two feeds.

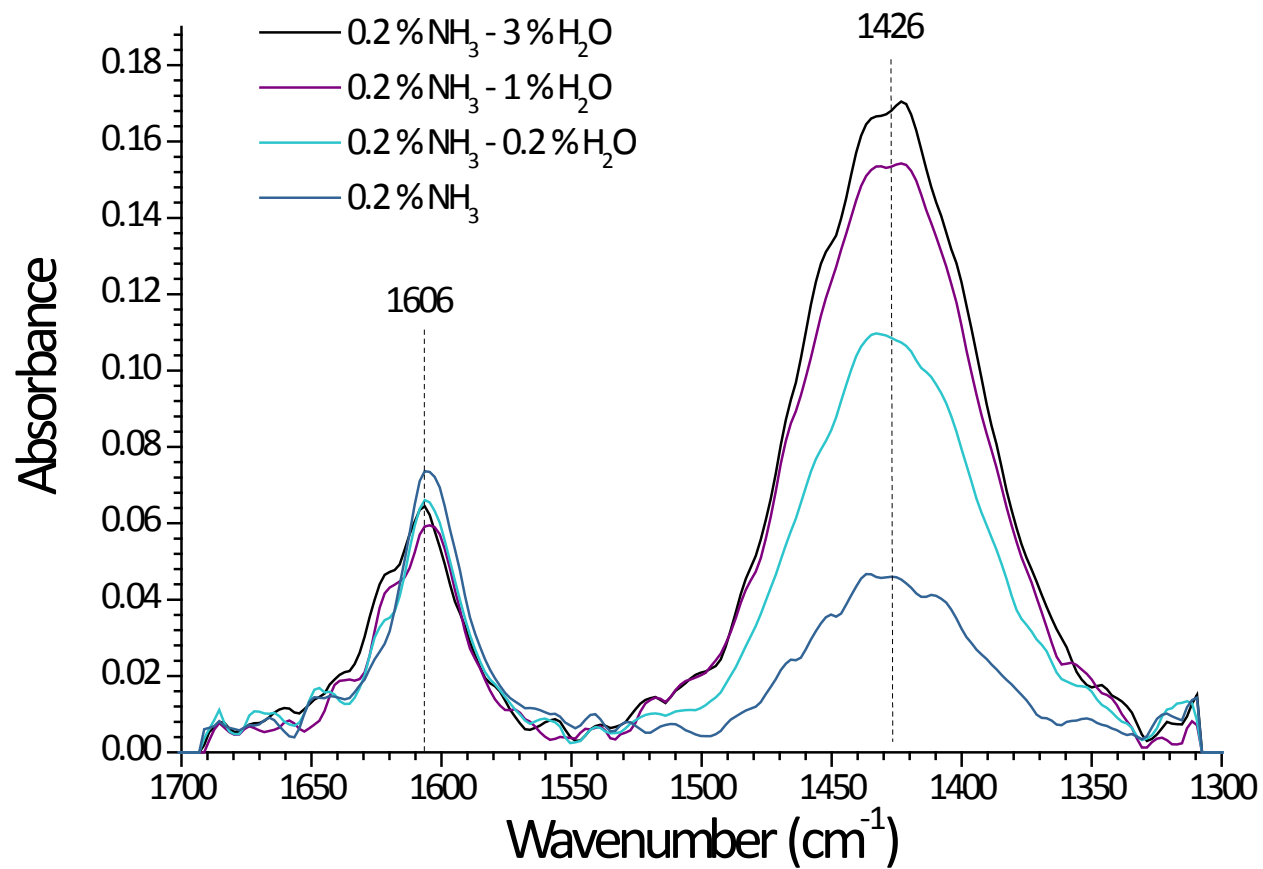


**Figure 9:** Evolution with the H<sub>2</sub>O partial pressure of the IR spectrum of 20.4%TiO<sub>2</sub>/SiO<sub>2</sub>-G recorded under different NH<sub>3</sub>/H<sub>2</sub>O/He flows at 200 °C after pre-treatment. The background corresponded to the spectrum recorded under He flow at 200 °C, mass of the pellet 30 mg.

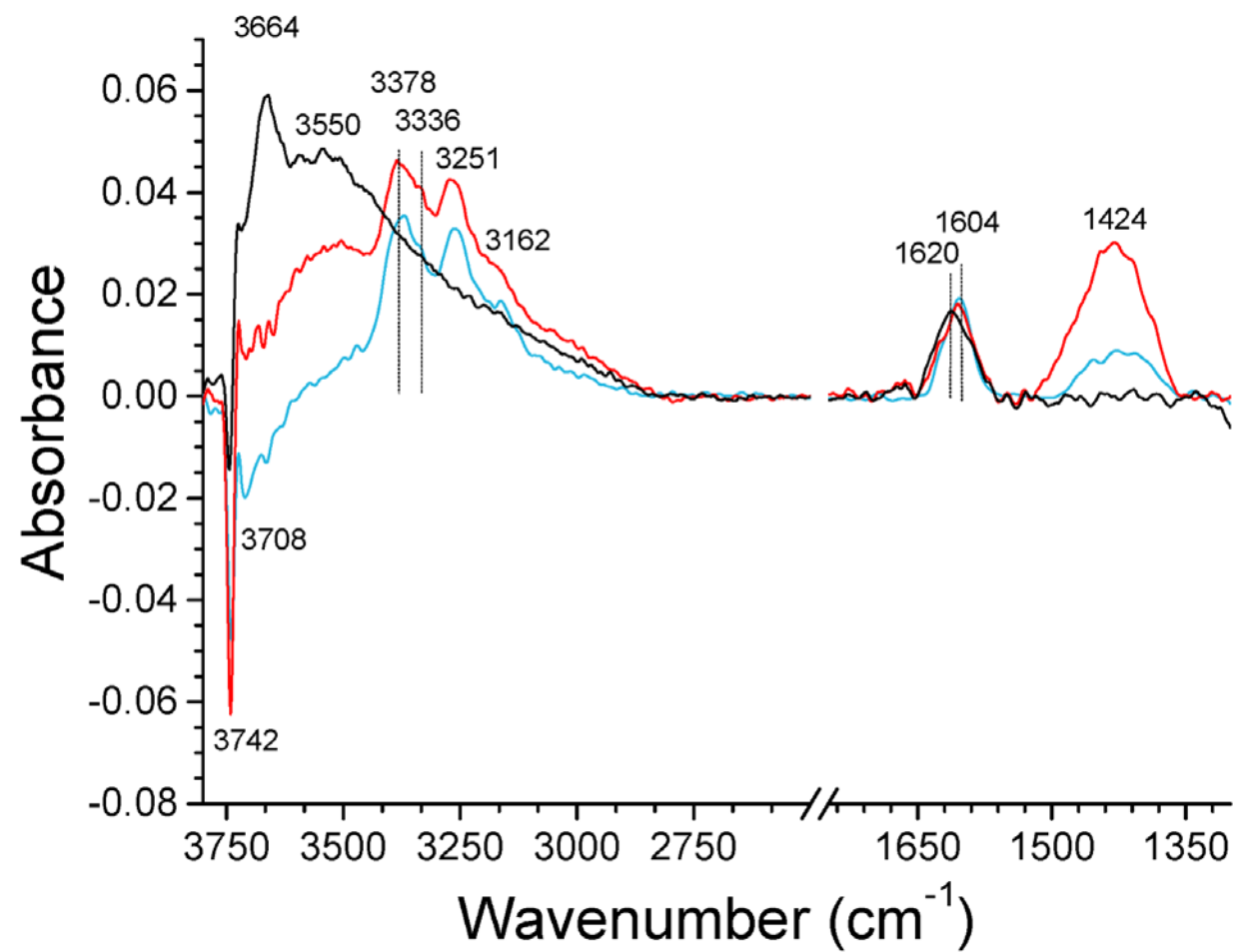


**Figure 10:** IR spectra of 19.5%TiO<sub>2</sub>/SiO<sub>2</sub>-A recorded under 3% H<sub>2</sub>O, 1% NH<sub>3</sub>, 3% H<sub>2</sub>O+1% NH<sub>3</sub> at 250 °C after pre-treatment. The background corresponded to the spectrum recorded under He flow at 250 °C, mass of the pellet 14 mg.

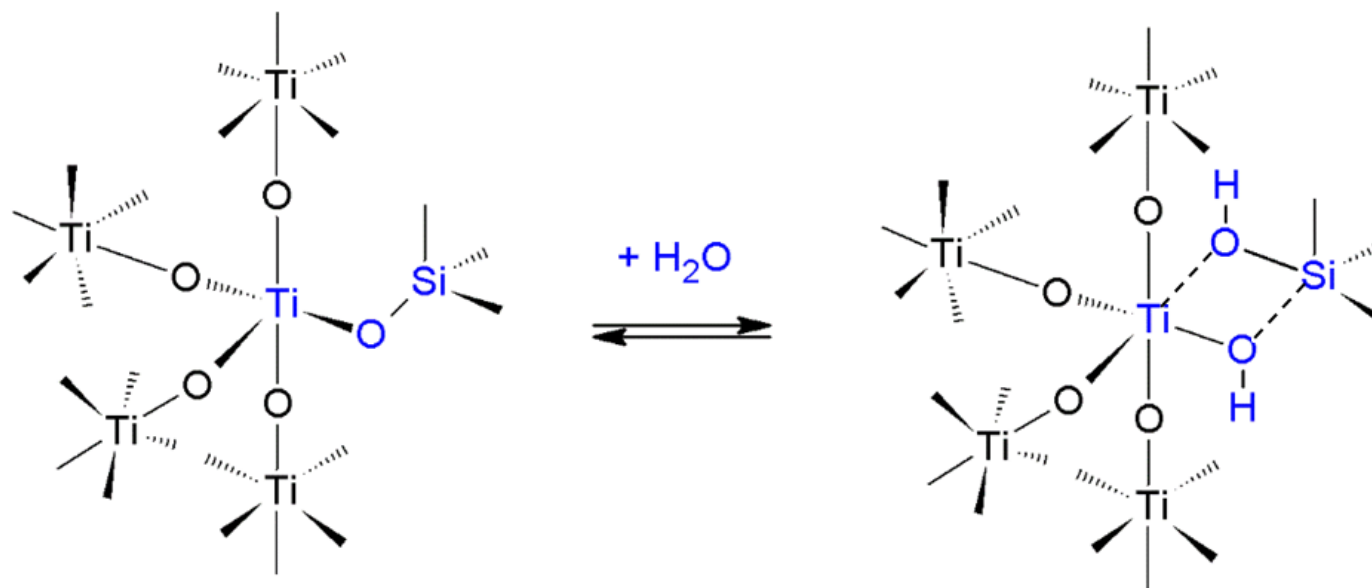


**Figure 11:** Hydrolysis scheme of Ti-O-Si bonds located at the interface between TiO<sub>2</sub> amorphous clusters and SiO<sub>2</sub> support. The pseudo bridging OH bonds corresponded to Brønsted acid sites leading to activity enhancement by addition of water vapor to the feed.